Research Article

Qiang Tong, Tao Jiao, Zhao Qi, Haihong Wang, Yicang Liu, Yushuang Zhu*, and Hanlin Liu

Spatiotemporal evolution of single sandbodies controlled by allocyclicity and autocyclicity in the shallow-water braided river delta front of an open lacustrine basin

https://doi.org/10.1515/geo-2020-0220
received September 17, 2020; accepted January 05, 2021

Abstract: The spatial and temporal evolution of the sandbody architecture of shallow-water deltas in open lacustrine basins is controlled by the classification of allocyclicity and autocyclicity. On the southwestern margin of the Ordos Basin, a braided river system deposited a shallow-water delta in the Late Triassic Period. Based on the principle of sequence stratigraphy and the hierarchical analysis of reservoir architecture, the spatial and temporal evolution of individual sandbodies in the Chang 8_1 member of the Yanchang Formation in the Zhenbei Oilfield is interpreted by utilizing data from cores, wells and outcrops. The research ideas are as follows: large deposition scale architectural elements (first- to third-order cycles, as defined by Miall) of different sequence levels are affected by allocyclicity associated with changes in tectonic activity, provenance, and sea level, and small deposition scale architectural elements (fourth- to fifth-order cycles, as defined by Miall) of different sedimentary facies mainly consist of individual sandbodies that are affected by autocyclicity associated with lake-level changes caused by various river processes. Based on previous studies, the results are as follows. The sedimentary characteristics of shallow-water deltas have been verified by core and outcrop data. In addition, three ultrashort-term cycles are identified on the basis of boundary sequences and lithofacies' sequences in the outcrop section of the Rui River, and three sedimentary evolution stages of the delta front are defined. Finally, according to well data, five types of architectural elements at the level of single sandbodies are identified. The vertical superimposition and lateral contact relationships of different architectural elements indicate that during the three sedimentary evolution stages, the hydrodynamics weakened, strengthened slightly, and finally weakened substantially. Among the 20 kinds of architectural element spatial combination patterns formed by single sandbodies, primary and secondary sandbodies have great potential for hosting remaining oil. In the process of architectural spatiotemporal evolution, the geometry and connectivity of the underwater distributary channel gradually weakened, and the spatial relationship between the underwater distributary channel and other architectural elements increased. This article proposes a new method for researching shallow-water deltas and has some guiding significance for exploiting the remaining oil in oil fields.

Keywords: shallow-water braided river deltas, allocyclicity, autocyclicity, single sandbody architecture, architectural element combination pattern, spatiotemporal evolution

* **Corresponding author: Yushuang Zhu,** Department of Geology, State Key Laboratory of Continental Dynamics, Northwest University, Xi'an, 710069, China, e-mail: nwugeology2lou@163.com
Qiang Tong: Department of Geology, State Key Laboratory of Continental Dynamics, Northwest University, Xi'an, 710069, China
Tao Jiao, Zhao Qi: Institute of Geology, No. 5 Oil Production Plant, PetroChina Changqing Oilfield Company, Xi'an, 710021, China
Haihong Wang: Institute of Geology, No. 7 Oil Production Plant, PetroChina Changqing Oilfield Company, Xi'an, 710299, China
Yicang Liu: Institute of Geology, No. 11 Oil Production Plant, PetroChina Changqing Oilfield Company, Xifeng, 745000, Gansu, China
Hanlin Liu: Department of Shale Gas, Research Institute of Petroleum Exploration & Development, PetroChina, Beijing, 100083; School of Earth and Space Sciences, Peking University, Beijing, 100871, China

1 Introduction

In 1885, Gilbert studied the sedimentary characteristics of a Pleistocene delta associated with Lake Bonneville and concluded that the delta exhibited an obvious three-layer structure comprising top set, fore set, and bottom set [1]. Later, scholars called this pattern a classic Gilbert-type delta. In the 1970s–1990s, to further understand the formation and evolution of deltas, many scholars performed extensive research work on a series of characteristics of deltas. Bogen studied deltas in several fjord lakes by geomorphology and sedimentology [2]. Syvitski and Farrow

compared two bayhead deltas from sedimentary structures, sediment character, and lithofacies [3]. Tye and Coleman studied the evolution of lacustrine deltas in Atchafalaya Basin [4].

However, because of the limitation of the three-layer structure of Gilbert deltas, the concept of the shallow-water delta was proposed. In 1960, Fisk divided river-controlled deltas into deepwater deltas and shallow-water deltas [5]. Postma classified deltas into shallow-water deltas and deepwater deltas and identified eight types of shallow-water deltas [6]. In recent years, research on shallow-water deltas has gradually deepened and widened. The research has included numerous aspects, including the formation dynamics, sedimentary microfacies, sedimentary models, and main control factors of shallow-water deltas [7,8].

In the past decade, the study of shallow-water deltas has developed further. For example, the division of sedimentary genesis related to underwater distributary channels has become more refined [9]. The stratigraphic slice method of seismic geomorphology has been gradually applied in this field [10]. The patterns of sandbody prediction, the formation of microfacies assemblages, and the sedimentary evolution process have been considered [11]. Although previous studies on shallow-water delta sedimentation are extensive, the main research directions remain focused on certain aspects, such as sedimentogenesis, texture type [12], sedimentary system evolution [13], geometry [14], and sedimentary characteristics and models [15].

On this basis, research concerning the architecture of sandbodies in shallow-water deltas has gained gradual attention [16] and has investigated the characteristics, main controlling factors and architectural patterns of various individual architectural elements [17], the remaining oil and heterogeneity [18,19], numerical simulations [20], etc. In contrast, little research has been performed on the sedimentary evolution process of architectural elements in shallow-water deltas or the evolution pattern of assemblage relationships between single sandbody architectural elements during the sedimentary evolution process. Since sedimentary evolution is accompanied by two types of cyclic mechanisms during strata formation, it is necessary to distinguish between allocyclicity and autocyclicity.

Allocyclicity is the product of changes in the balance between accommodation and sediment supply (A/S value) induced by changes in the sediment supply, tectonic subsidence, and sea level. It usually controls the stacking pattern of strata and forms a base-level change cycle. Autocyclicity only controls the internal structure of sedimentary facies in a sequence and the proportion of lithofacies, which is local or not regular. In particular, the formation of autocyclicity in fluvial sediments is mostly related to changes in hydrodynamic conditions.

More importantly, oil fields have faced conflicts in development and production due to heterogeneity in single sandbody architecture and reservoir interiors. Hence, this study is imperative to further depict the architectural sequence of shallow delta fronts, clarify the evolution of their single sandbody architectural elements, and analyze their spatial combination relationships and the factors controlling the remaining oil formation and distribution.

2 Geological setting

As a significant sedimentary basin in China, the Ordos Basin is rich in geological resources (Figure 1a). Additionally, the Upper Triassic Yanchang Formation, an important oil-bearing formation in the Ordos Basin, was deposited in a large open lacustrine basin [21], and the depositional system included rivers, lakes, and multiple deltas; the resulting deposits are the primary Mesozoic targets of exploratory development in the basin [22]. On the southwestern basin margin in the Ordos Basin, the Longdong area (eastern Gansu) is located on two first-order tectonic units that present a west-dipping monoclinal trend, and the area contains multiple lithologic-structural oil reservoirs (Figure 1b).

It has been pointed out that the sedimentary system of the Triassic Yanchang Formation in the Longdong area involved a shallow-water braided river delta with sediment delivered from the southwest direction [23,24]. The Longdong area was close to the southwestern provenance, and braided river deposits easily entered the lake directly, forming a deltaic depositional system. The sedimentary thickness of the Chang 8 Formation in the Ordos Basin is laterally stable, and there is no obvious regional steep slope belt in the lacustrine basin. In addition, the terrain is very gentle, and the slope angle is approximately 0.1° [25]. Thus, the structural foundation of the basin was favorable for the development of shallow-water deltas.

In general, under a combined supply from the Longxi Ancient Land to the southwest and the Qingling and Qilian Fold Belt to the south, a sedimentary environment involving a small delta plain and a shallow-water braided river delta with a large delta front developed in the Longdong area [24] (Figure 1c).

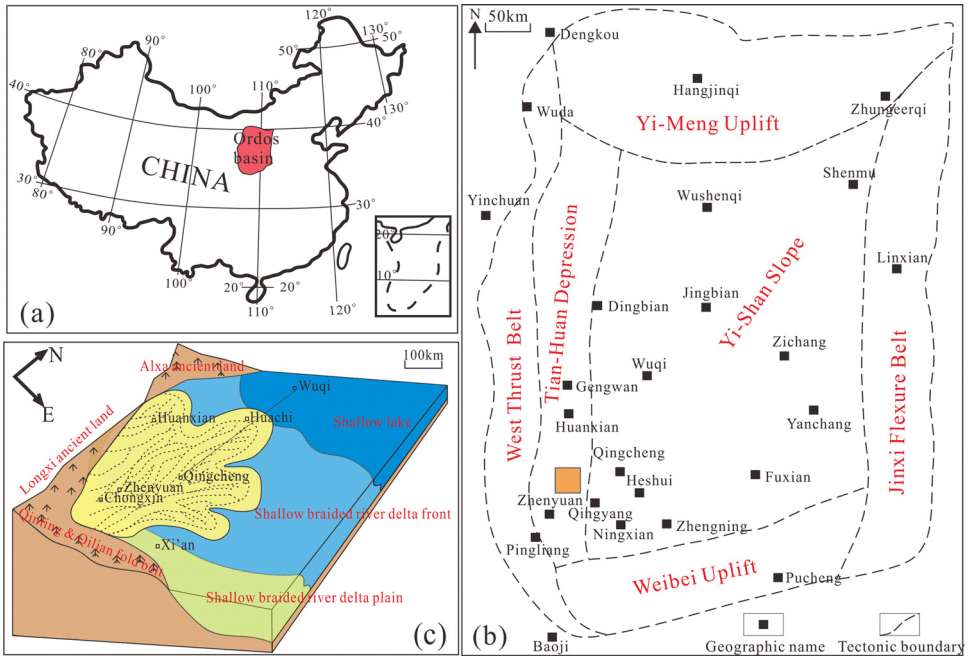

Figure 1: (a) The location of the Ordos Basin on a map of China; (b) location of the study area; (c) the shallow-water delta sedimentary model (modified from ref. [24]).

3 Samples and methods

On the basis of surveying extensive previous findings, this article studies the Chang 8_1 layer in the Yanchang Formation in the Zhenbei Oilfield, which is located in the Longdong area of the Ordos Basin, by relying on substantial well-logging data from closely spaced wells separated by approximately 300 m (Figure 2). These well data are supplemented by substantial outcrop profile observations along the Yan River and Rui River, additional core data, and considerable data on production performance in the oil field development process.

Initially, combined with the previous research results, the fourth- and fifth-order sequences as defined by Vail are identified by sequence stratigraphy theory, and these sequences correspond to the medium- and short-term sequences defined by Cross in high-resolution sequence stratigraphy.

Due to the lack of seismic data for the Yanchang Formation in the Ordos Basin, this article mainly uses abundant core observations and fine-scale logging analysis data to identify sequence boundaries. In the core, we can observe certain sedimentary structures near the sequence boundaries, such as the lag at the bottom of a river channel, scouring structures, contemporaneous mud gravel, calcareous layers, plant detritus, carbon dust, and vertical bioturbation burrows. Additionally, the logging response characteristics of sequence boundaries are obvious and include sudden increases in spontaneous potential (SP) and gamma ray (GR) values, increases in the negative anomaly amplitude, sudden increases in the deep and shallow lateral resistivity (RT) curves, etc., which are reflections of changes in the sedimentary environment. These responses are superimposed at boundaries.

In addition, in sandstones, changes in the grain size, thickness, and sand–mud ratio can also be used to identify sequence boundaries. After a sequence boundary is identified, the single sandbody configuration interface is identified on the basis of logging curve characteristics. The architectural interface can be distinguished effectively by using the electrical characteristics of the SP curve, natural GR curve, RT curve, and acoustic time difference (AC) curve.

The short-term and ultrashort-term cycles in allocyclicity can be identified by sequence boundaries. Furthermore, first- and second-order autocyclicity can be identified by using the architectural interface of a single sandbody, and these elements correspond to the fourth- and fifth-order architectural elements defined by Miall [26–28], respectively. Finally, a complete architectural element division scheme from the sequence stratigraphic level to the single sandbody level is formed.

Notably, the identification of sequence stratigraphy architectural bounding surfaces is a leading step. For

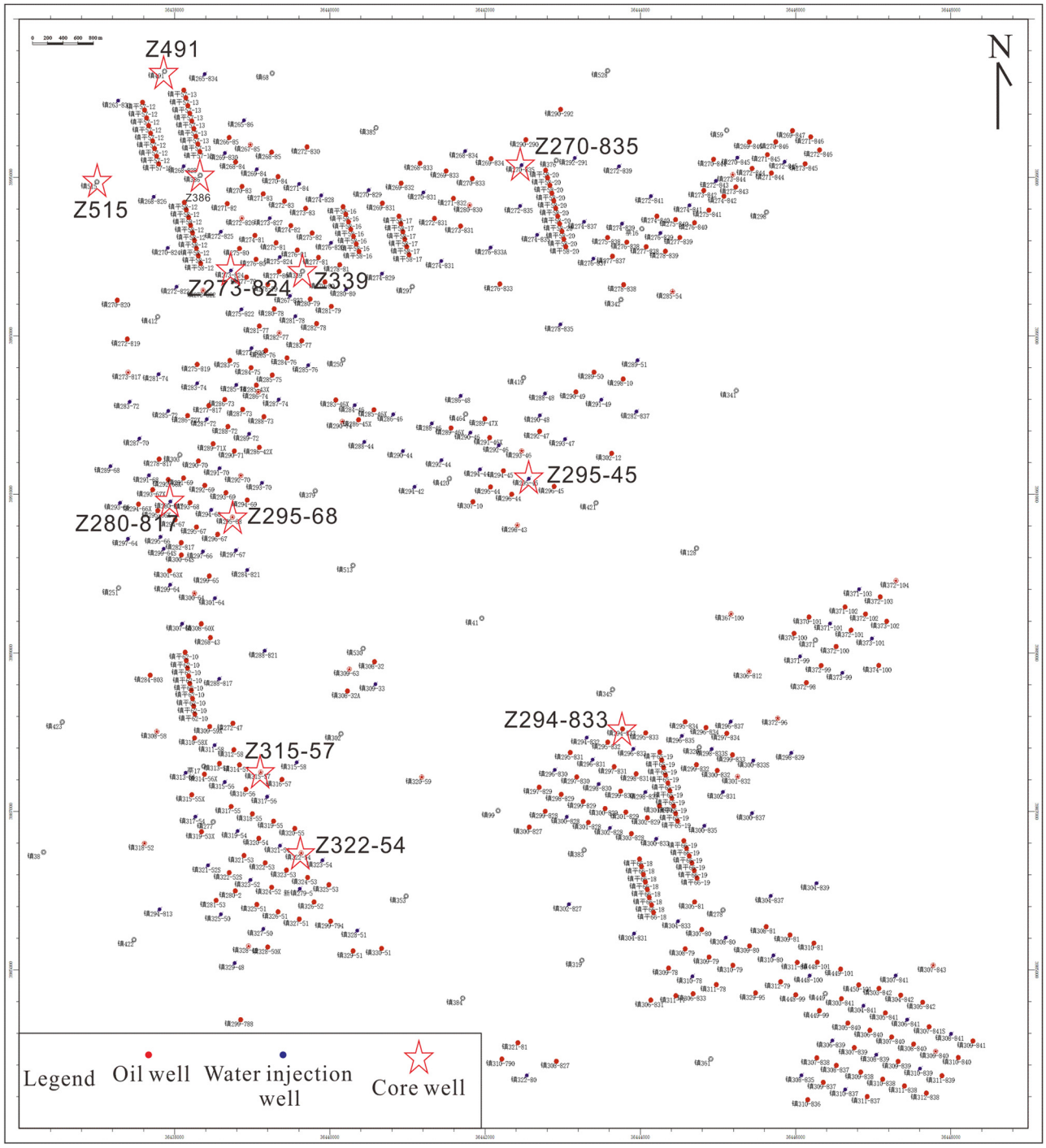

Figure 2: Well locations and coring well locations in the study area.

allocyclicity, the base-level cycle-based partitioning method in the high-resolution sequence stratigraphic division is still used. For autocyclicity, the architectural boundaries are identified on the basis of comprehensive lithology–electricity curves. The present sequence architecture partitioning scheme not only takes into account the isochronism of high-precision sequence division but also adopts the hierarchy of architectural research.

Afterward, based on the study of the sedimentary characteristics of shallow-water deltas, the relative lake-level changes are studied by analyzing the lithofacies and logging, and the results are used to establish

the evolution process over time. Finally, combined with the results of architectural element identification, the evolution characteristics of spatial morphology are formed, and a complete evolution model of architectural elements is established.

4 Sedimentary characteristics of a shallow-water braided river delta

4.1 Evidence of shallow-water delta deposition

According to the current views in shallow-water delta sedimentation research, the sediments forming the reservoirs experienced long-distance transport by the action of traction currents and have low compositional maturity, moderate textural maturity, and overall fine granularity, with most deposits being fine sandstones [29].

A large number of core data confirm that the study area was characterized by a shallow delta front depositional environment. First, the fine-grained deposits are dominantly fine sandstone and siltstone (Figure 3a and b). Second, the sandstone is mainly gray, gray green and gray white, and the mudstone is mostly dark gray and gray black (Figure 3c and i). A large number of sedimentary structures of strong hydrodynamic origin can be seen, such as parallel bedding, trough bedding, planar cross bedding, and retention deposition (Figure 3c–f). Wedge bedding, sand grain cross bedding, and horizontal bedding can also be seen, reflecting a relatively weak sedimentary environment (Figure 3g, h, and k). Importantly, a large number of broken rhizome and leaf fossils in the mudstone are signs of a shallow-water sedimentary environment, such as a shore or shallow lake (Figure 3o and n). Also, the wavy bedding is formed under oscillatory hydrodynamic conditions, which is the reflection of the rapid change of lake waves in shallow-water delta (Figure 3l). Worm burrows are present in the mudstone, indicating that the lake was shallow, the underwater sedimentary environment was turbulent, and the oxygen level was sufficient (Figure 3p). Finally, thin coal beds and carbonaceous mudstones are common (Figure 3j, m, and n), reflecting a shallow-water environment in the Longdong area. In response to lake-level fluctuations, subaerial and subaqueous sedimentary environments appear to alternate. These core observations suggest that the study area mainly featured a delta front sedimentary environment impacted by frequent lake-level fluctuations.

Changes in the lake level can induce changes in redox reactions, migration of ancient lake shorelines, and distinct rhythms in shallow-water sedimentation. The observed sedimentary sandbodies are diverse in form. Among them, sandbodies at the delta front mouth bar exhibit restricted development. The underwater channels bifurcated and diverted frequently, creating deposits that are superimposed vertically and horizontally, extend long distances, and are large in scale. Additionally, sandbody development was influenced by the base-level elevation and subsidence, and accretion and retrogradation occurred frequently, thereby leading to diverse sandbody combinations, complex spatial overlap and contact relationships, numerous sandbody architectural elements, complicated horizontal and vertical combination relationships, and prominent associations between spatiotemporal evolution and base-level cycles.

4.2 Characteristics of sequence stratigraphy

At present, the Yanchang Formation is mainly divided into five long-term base-level cycles, and a high-resolution sequence stratigraphic framework with medium-term base-level cycles as the unit have been established. The transition surface between long-term base-level cycles LSC2 and LSC3 is located between Chang 8_2 and Chang 8_1 (Figure 4). Additionally, Chang 8_2 is a complete medium-term cycle known as MSC2-III, and Chang 8_1 is an ascending half cycle of the medium-term cycle known as MSC3-I [30].

The medium-term base-level cycle is controlled by the long-period eccentricity of the Milankovitch cycle. This cycle is usually bounded by a large-scale scouring surface and consists of a series of short-term base-level cycles. Due to the limitation of the vertical resolution of seismic data, it is difficult to identify the interface of medium-term cycles on seismic profiles. Therefore, this article uses outcrops, logging curves, and lithologic profile characteristics to identify it.

MSC3-I is equivalent to the Chang 8_1 member. The medium-term cycle consists of a series of short-term cycles dominated by rising base-level cycles. MSC2-III is equivalent to the Chang 8_2 member and consists of a complete short-term cycle. The Lijiapan shale at the top of Chang 9 effectively indicates the boundary with Chang 8 (Figure 5a). Furthermore, the SB3 interface is the bottom interface of LSC3, which is roughly equivalent to the interface between Chang 8_2 and Chang 8_1 (Figure 5b). Additionally, this interface is a microfacies transition

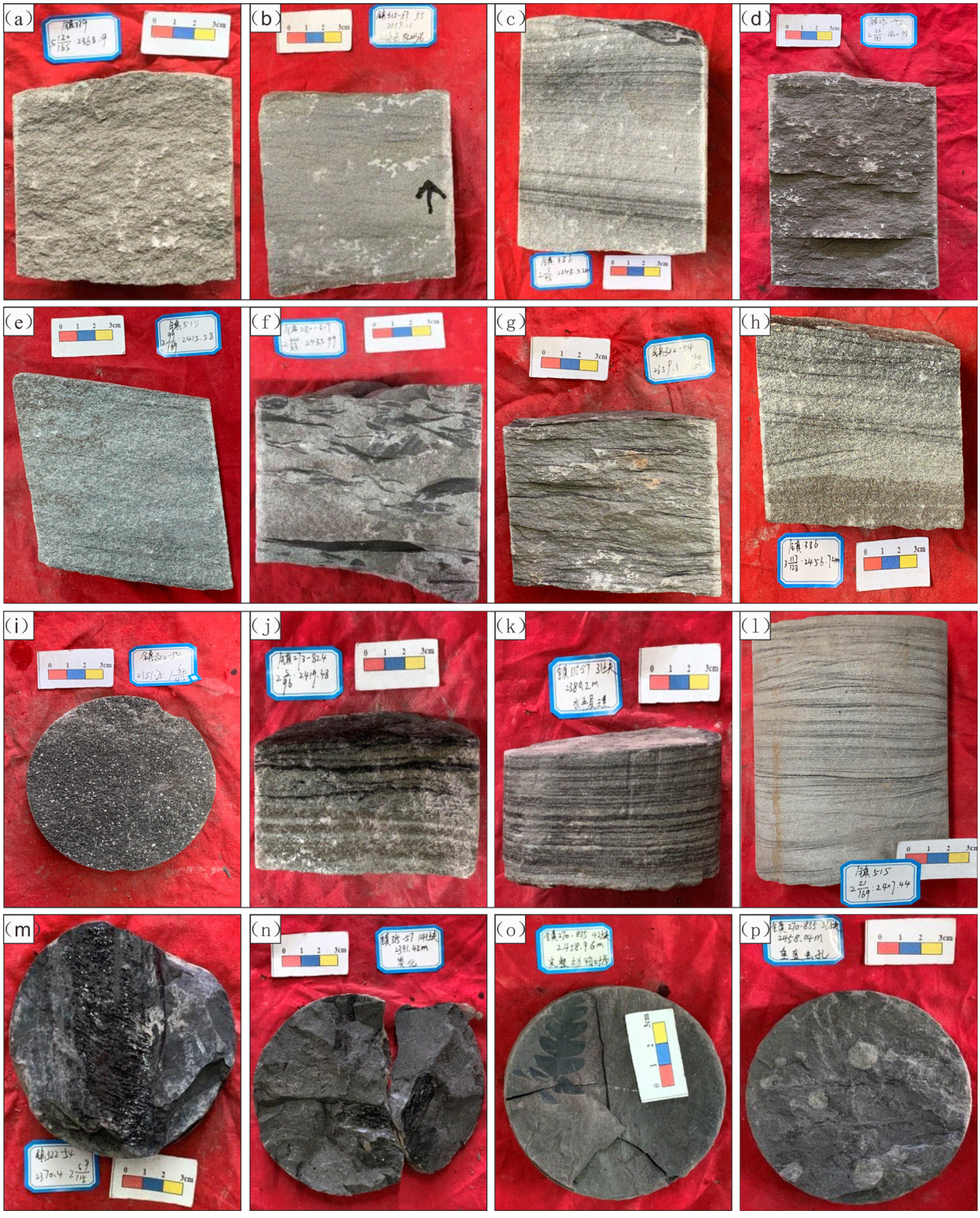

Figure 3: Sedimentary indicators of a shallow-water delta. (a) Fine sandstone; (b) siltstone; (c) parallel bedding; (d) trough bedding; (e) planar cross bedding; (f) retention deposition; (g) sand grain cross bedding; (h) Wedge bedding; (i) mudstone; (j) thin coal beds; (k) horizontal bedding; (l) wavy bedding; (m) carbonaceous mudstones; (n) carbonaceous plants; (o) broken rhizome and leaf fossils; (p) worm burrows.

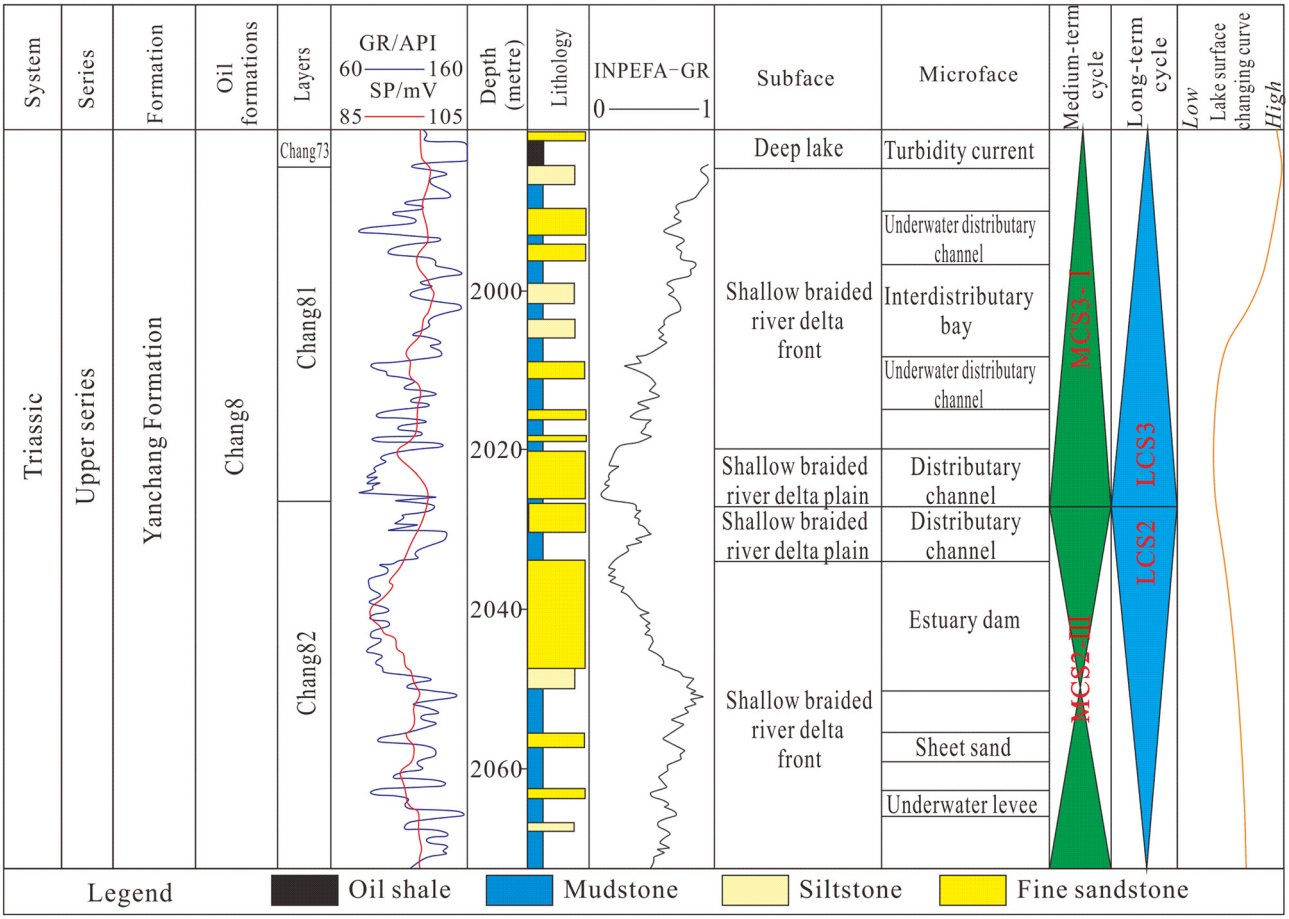

Figure 4: Sequence stratigraphy in the Chang 8 layers of the Yanchang Formation.

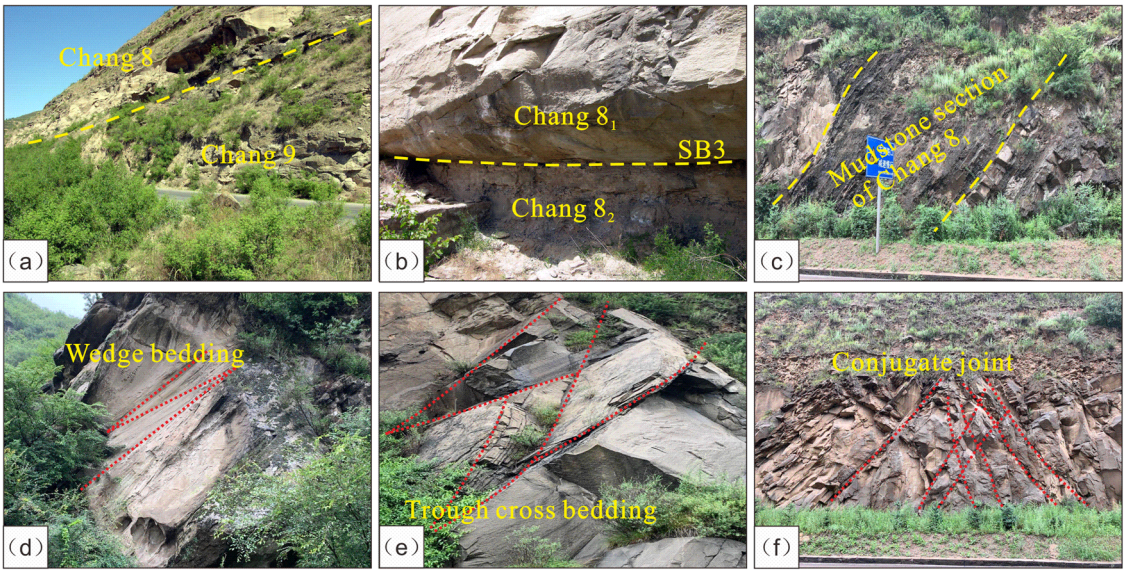

Figure 5: Identifying marks of sequence stratigraphy in outcrop sections along the Yan River and Rui River. (a) Boundary of Chang 8 and Chang 9 in Yan River; (b) SB3 interface of LSC3 in Yan river; (c) microfacies transition surface in Rui river; (d) large trough cross bedding in Rui River; (e) wedge bedding in Rui River; (f) conjugate joints in distributary channel in Rui River.

surface that formed during continuous deposition (Figure 5c). The lithology of the Chang 8_2 layer is light gray calcareous fine sandstone, and the lithology of the Chang 8_1 layer is pebbly sandstone. The outcrop profiles are characterized by large distributary channels, showing large trough and wedge cross bedding (Figure 5d and e). In addition, conjugate joints can be seen in the distributary channel (Figure 5f).

Similarly, the changes in natural GR and RT curves can be used to effectively identify short-term or ultrashort-term cycles. For example, the change from low to high natural GR values reflects an increase in the proportion of shale, which can represent a short-term positive cycle or ultrashort-term positive cycle.

4.3 Characteristics of lithofacies

Based on the identification of sequence boundaries, the high-frequency sequence in the Chang 8 Formation in the outcrop section along the Rui River is studied, and three ultrashort-term base-level cycles are identified in the Chang 8_1 Formation (Figure 6).

Based on these three ultrashort-term cycles, the lake-level and hydrodynamic intensity changes during the sedimentary evolution of the Chang 8_1 Formation are studied. The hydrodynamic intensity decreased from high to low in the third ultrashort cycle. In the second ultrashort-term cycle, it changed from low to high. In the first ultrashort-term cycle, it changed from high to low again. This pattern indicates that the lake level experienced three trends: rising, falling, and rising.

First, a series of marks of lithofacies were identified in the outcrop profile. Then combined with the analysis of indicators of lithofacies and logging curves, the facies associated with this sedimentary evolution stage in the study area were differentiated, and 10 sequences of lithofacies in each ultrashort-term cycle were identified. The results show that sequence changes in the lithofacies reflect changes in the lake level, and the identified changes were used to describe the sedimentary evolution process (Figure 7).

In the first phase, a medium-thick fine sandstone facies with large cross bedding is common, and occasional thin layers of wavy-bedding siltstone facies and horizontally bedded mudstone facies are observed. Normal cycles are quite common and reflect strong hydrodynamic forces and good sandbody development under the sedimentary environment in this phase. The sandbodies are dominantly underwater distributary channel sandbodies, and a few underwater natural levees are present. In addition, the fine-grained sedimentary part developed in the interdistributary bay.

In the second phase, reverse cycles with an inverted tapered shape appear, and these deposits are composed of multiple lithofacies. Additionally, parallel bedding and various cross beddings indicate strong hydrodynamic conditions. In addition, sand ripples indicate medium hydrodynamic conditions, and the wavy bedding indicates an oscillating depositional environment associated with well-developed sandbodies. It is considered that these deposits represent estuary dam and front sheet sand microfacies and appear above the three types of sedimentary microfacies in the first phase. Moreover, the many estuary dams almost form a skeleton sandbody in this phase jointly with the underwater distributary channels. Additionally, the number of underwater natural levees increases remarkably, the number of fine-grained interdistributary bay sedimentary units decreases, and sheet sands are developed in small amounts in extremely limited areas.

In the third phase, the reverse cycles disappear, and the normal cycles associated with underwater distributary channels become dominant again. It is speculated that the sandbodies associated with estuary dams and underwater distributary channels decrease in number, and the underwater distributary channel sandbodies remain as sedimentary skeletal sandbodies. In addition, the sheet sands grow greatly, the underwater natural levees lessen in number, and the fine-grained sedimentary units of the interdistributary bay grow in number again.

5 Results

5.1 Architecture classification scheme controlled by base-level cycles in the study area

Since the identification of architectural elements at the sequence stratigraphic scale has been completed on the basis of sequence boundary identification, the following is mainly focused on the architectural elements under the influence of autocyclicity [31]. Based on Miall fluvial facies architectural element analysis method [26], this article describes the architectural interfaces of the third, fourth, and fifth levels, thus completing the division of architectural elements of each level (Table 1).

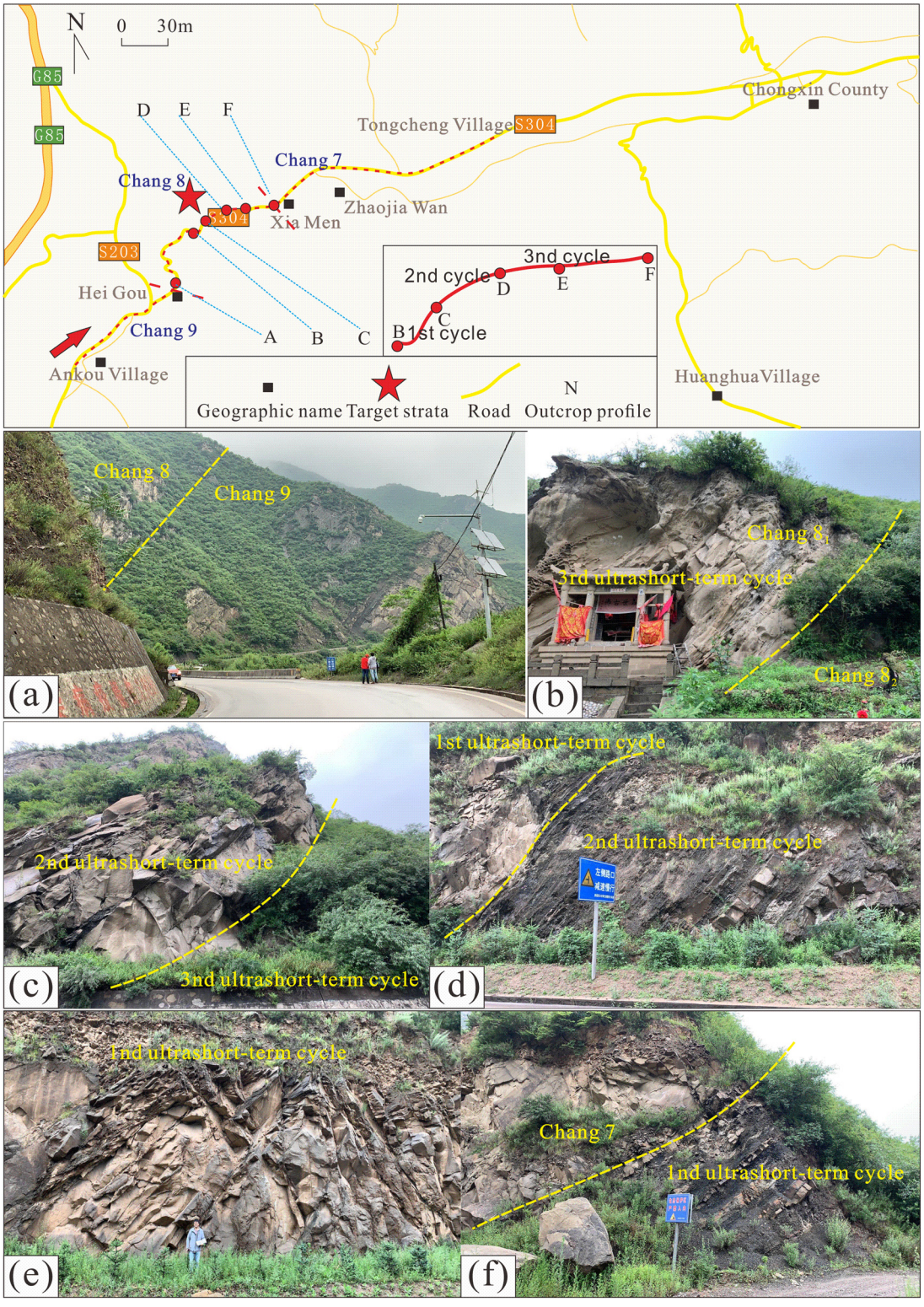

Figure 6: Three ultrashort-term cycles in the Chang 8_1 outcrop section along the Rui River. (a) The boundary of Chang 8 and Chang 9; (b) the bottom of 3rd ultrashort-term cycle; (c) the bottom of 2nd ultrashort-term cycle; (d) the bottom of 1st ultrashort-term cycle; (e) the middle of 1st ultrashort-term cycle; (f) the top of 1st ultrashort-term cycle.

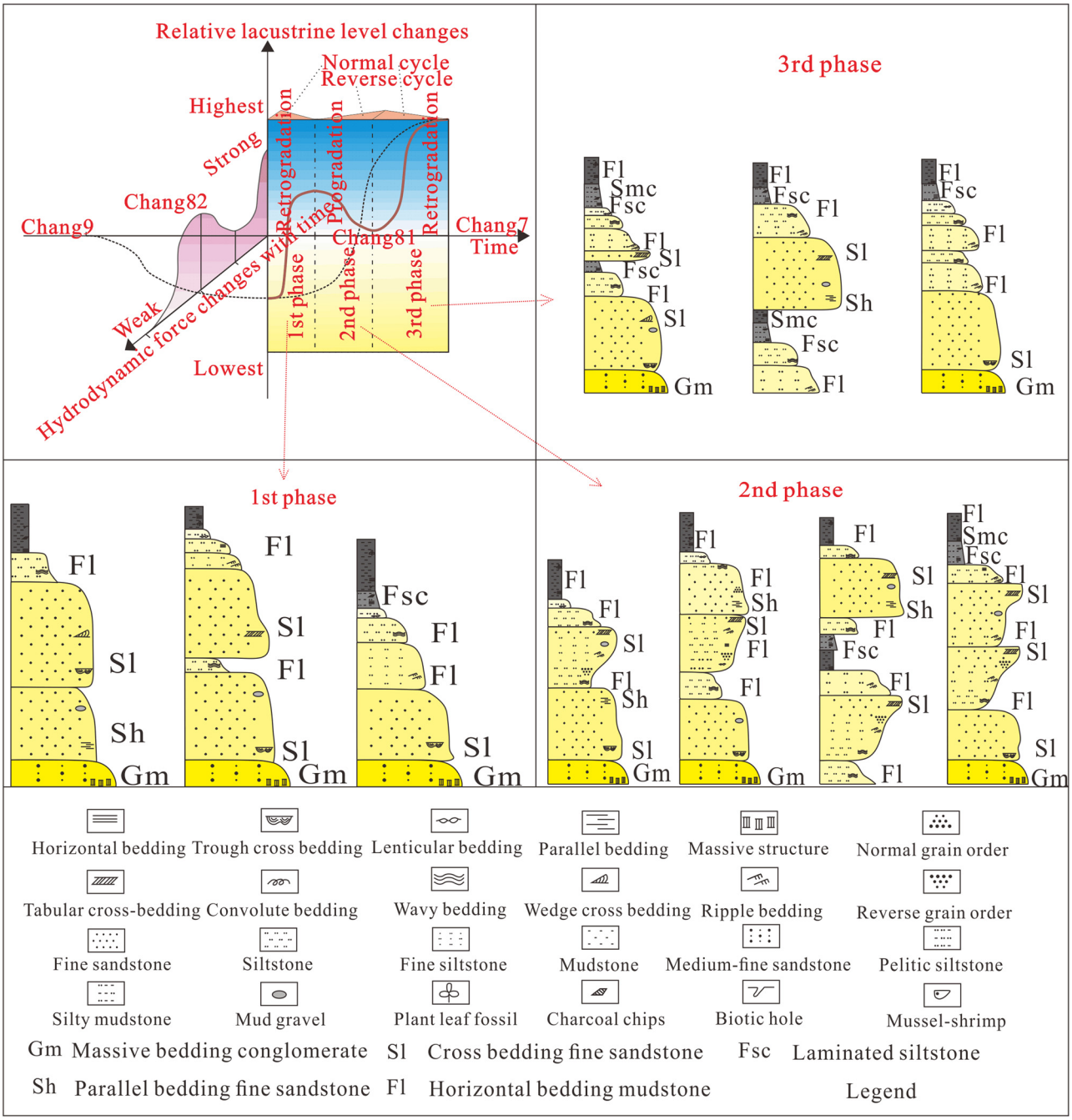

Figure 7: Lithofacies' sequence of the three ultrashort-term cycles in the Chang 8_1 outcrop section.

5.2 Identification of single sandbody architectural element boundaries

In view of the necessity of single sandbody research, we need to further subdivide the fifth- to third-order bounding surfaces of Miall, under whose constraints, various orders of autocyclicity have been formed. The boundary of first-order autocyclicity is the same as the boundaries of the ultrashort-term cycles, which are mostly erosion or flooding surfaces, and it can be identified from the retention deposition at the bottom of the core and the abrupt change in the natural GR curve in the logging response. The architectural elements of this level reflect a mobile distributary channel sandbody complex comprising multiple individual sandbodies or a plant leaf complex formed by a single distributary channel. The

Table 1: Architectural element partition scheme from allocyclicity to autocyclicity (modified according to [26,31])

Miall's hierarchy	Sequence architecture boundary classification	Sequence architecture boundary type	Conventional sequence stratigraphic classification	Base-level cycle classification	Sedimentogenesis	Limited stratigraphic unit	Limited sedimentary unit
Eighth order	Third-order sequence boundary	Unconformable discontinuity and its corresponding conformable surface	Sequence	Long-term base-level cycle	Tectonic movement and relative changes in lake level	Formation (oil-bearing series)	Basin filling body
Seventh order	Fourth-order sequence boundary	Sediment pattern changing boundary	Parasequence set	Medium-term base-level cycle	Relative changes in lake level	Section (oil layer group)	System tract
Sixth order	Fifth-order sequence boundary	Boundary of characteristic sedimentary environment	Parasequence	Short-term base-level cycle	Periodic changes in hydrodynamic conditions	Subsection (sands group/ small layer)	Vertically superimposed bodies of valleys or multiphase river delta sediments
	Sixth-order sequence boundary	Minimum allocycle boundaries, such as lake flooding surface	Layer set	Ultrashort-term base-level cycle	Lake flooding surface	Layer (single layer)	Single-phase river delta sedimentary bodies
Fifth order	First-order autocycle boundary	Boundaries with changes in features like granularity and bed form scale that are corresponding to the maximum autocycle	Layer	First-order autocycle	Migration or erosion of distributary channel complex	Single sand layer	Mobile distributary channel sandbody complex, lobe complex formed by a single distributary channel
Fourth order	Second-order autocycle boundary	Lateral migration of sedimentary bodies, etc., erosion surfaces		Second-order autocycle	Migration or erosion of single sandbodies associated with lake level fluctuations		Single sandbody level, mobile distributary channel single site dams, fixed single distributary channels, and single estuary dams
Third order	Third-order autocycle boundary	Hydrodynamic condition differential surfaces, without apparent, time discontinuity or erosion		Third-order autocycle	Changes in medium-term hydrodynamic conditions associated with turbulence or migration of water bodies that cross or surround the channel bed forms		Accretion bodies, lateral accretion layers, lateral accretion bodies of foreset beds

boundary of second-order autocyclicity is mostly erosion surfaces resulting from lateral migration of sedimentary bodies. They control the migration or erosion of individual sandbodies related to lake wave fluctuations, and individual sandbody architectural elements should be constrained. Third-order autocyclicity boundaries generally represent the differential surfaces of hydrodynamic conditions. They restrict the formation of lateral accretion and accretion in single sandbodies.

Due to the influence of the 3- to5-level architectural interface on the connectivity of the single sandbodies, during the development stage of an oil field, the third- to fifth-level architectural interface can be identified as a seepage barrier. The boundary orders are equivalent to the corresponding orders of architectural elements.

Depending on genesis, three types of interlayers are identified by using well data from the study area, namely, muddy, calcareous, and physical property interlayers (Figure 8). Muddy interlayers are common, while calcareous interlayers and physical seepage barriers are mostly in the form of interlayers (Table 2).

From the table above, it is clear that the GR and AC curves are remarkably effective in identifying the three types of seepage barriers. When supplemented by the SP curve and RT curve, a semiquantitative effect for architectural bounding surface identification can be achieved.

5.3 Base-level cycle identification and classification for single-well sequence stratigraphy architecture

By using the above method, 6 first-order autogenetic cycles and 10 second-order autogenetic cycles were identified in well Z339 (Figure 9).

As shown in the figure, two obvious large changes can be seen in the natural GR curve. These changes are associated with very high values, which reflect muddy deposition after the end of channel sandbody deposition. These cycles reflect three channel sedimentation processes and correspond to the three ultrashort-term cycles in the outcrop profile. Each instance in which the natural GR curve increases and the AC curve decreases to a low value corresponds to a change in the sedimentary environment. All of these factors represent discontinuities in

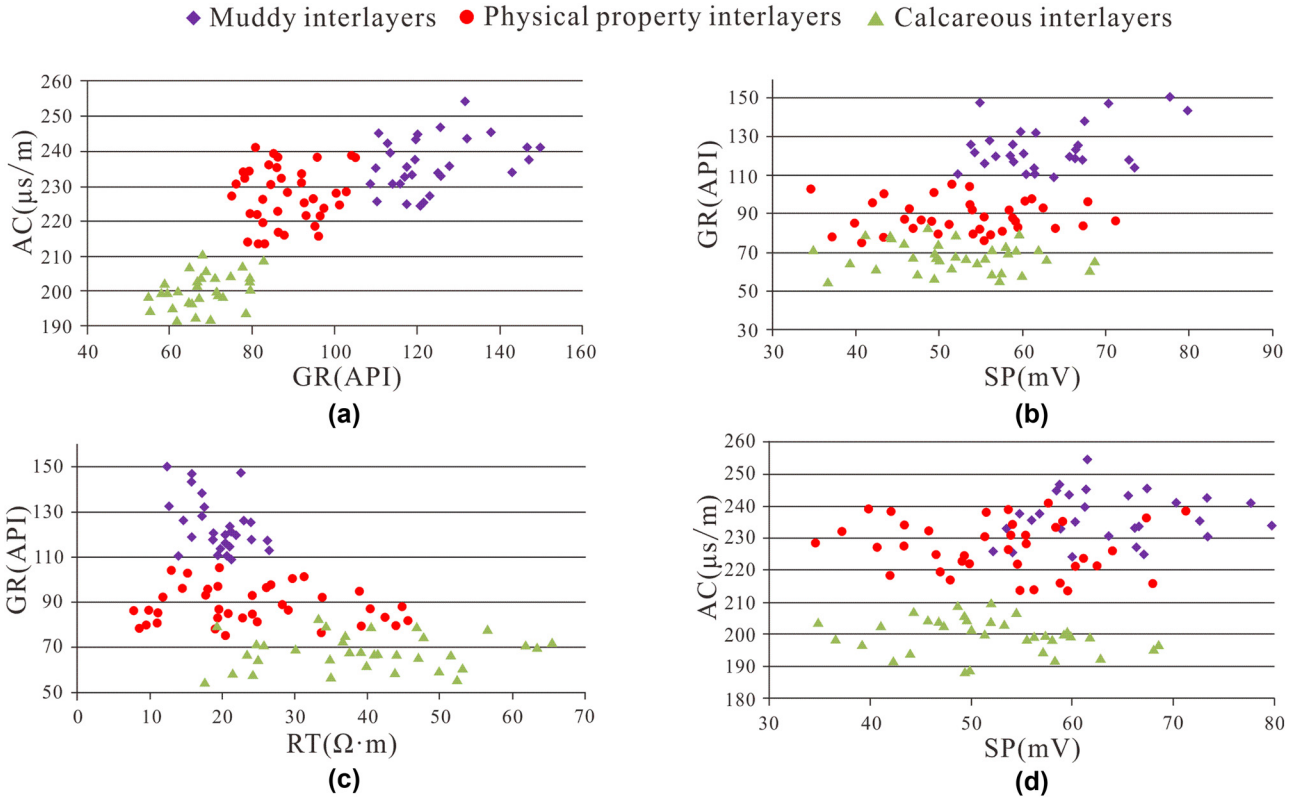

Figure 8: Identification of third- to fifth-order architectural element interfaces by using lithological-electrical response characteristics (a) AC-GR lithological-electrical response; (b) SP-GR lithological-electrical response; (c) RT-GR lithological-electrical response; (d) SP-AC lithological-electrical response.

Table 2: Lithological-electrical characteristic response statistics of third- to fifth-order bounding surfaces in the study area

Architecture boundary type	Lithology	Development sites	Logging curve characteristics	Genesis	Value ranges and means of logging curves			
					SP (mV)	GR (API)	RT (Ω l)	AC (μs/s)
Calcareous interlayer	Calcareous mudstone, calcareous fine siltstone	Top and bottom boundaries of channel sandstone, sites with easy formation of diagenetic cementation bands at the architecture boundaries	High resistivity, low acoustic wave, low spontaneous potential, low gamma	Mainly diagenesis	34.9–68.7 52.1	54.8–82.7 67.8	17.7–65.6 39.7	188.4–210.1 199.8
Argillaceous interlayer	Mudstone, silty mudstone	Between two genetic sandbodies, channel migration edges, lateral accretion sites	Low resistivity, high acoustic wave, hole enlargement, high spontaneous potential, high gamma, highly argillaceous	Mainly sedimentation	52.2–79.9 63.3	108.9–150.1 123.6	12.6–26.6 19.6	224.3–254.1 236.3
Physical property interlayer	Oil-stained sandstone, siltstone, muddy conglomerate	Lag sedimentation sites at the river bottom, rapid sedimentation sites like river channel edges and landslides	Microelectrode logging curve presents certain amplitude differences, and the resistance, acoustic wave, spontaneous potential	Possessing certain porosity and permeability, which is tough to reach	34.6–71.2 52.7	75.1–105.2 88.4	7.7–45.7 24.1	213.5–241 227.3

the sandbody continuity and the formation of an architectural interface. The division of second-order autogenetic cycles is also based on the above characteristics of the lithological-electrical responses, so it will not be described in detail.

The architectural elements of a single sandbody correspond to each level of autogenetic cycles. Miall's fifth-order bounding surfaces depict a sandbody complex that is represented by single sedimentary microfacies in the river delta context. Furthermore, a single sandbody represented by the single sedimentary microfacies constitutes the key architectural elements discussed in this article, which are depicted by the fourth-order boundaries, such as the single underwater distributary channels and single estuary dams.

5.4 Precise characterization of sedimentary system evolution by the three ultrashort-term base-level cycles

In the present research setting, the single sandbodies in the river delta sedimentary system are the minimum unit of time span under autocyclicity, and the architectural elements of the level represent the beginning and the end of changes in the river delta sedimentary evolution. Especially in the sedimentary environment of the shallow-water delta front, the variation range of water depth is small. Thus, large-scale architectural elements cannot accurately describe ultrashort-term changes, and extremely high-frequency lake-level changes are also unclear. These results indicate that the shorter the base-level cycle process, the higher the accuracy of architectural element characterization. Hence, the precise characterization of sixth-order sequence boundaries (lake flooding surfaces) offers the most accurate guidance for research on sedimentary system evolution.

Given the differing features of single-phase river delta sedimentary bodies above and below base level, we subdivided the shallow braided river delta front sedimentary systems in the study area in sequential order into three ultrashort-term cycle phases: the shallow braided river upper delta front sedimentary system, the shallow braided river middle delta front sedimentary system, and the shallow braided river lower delta front sedimentary system.

In essence, the architectural elements depicted by autocyclicity are the facies architecture. Therefore, it is necessary to establish relationships between autocyclicity and various orders of facies architectural elements based on well data (log lithofacies). Finally, an integration of the

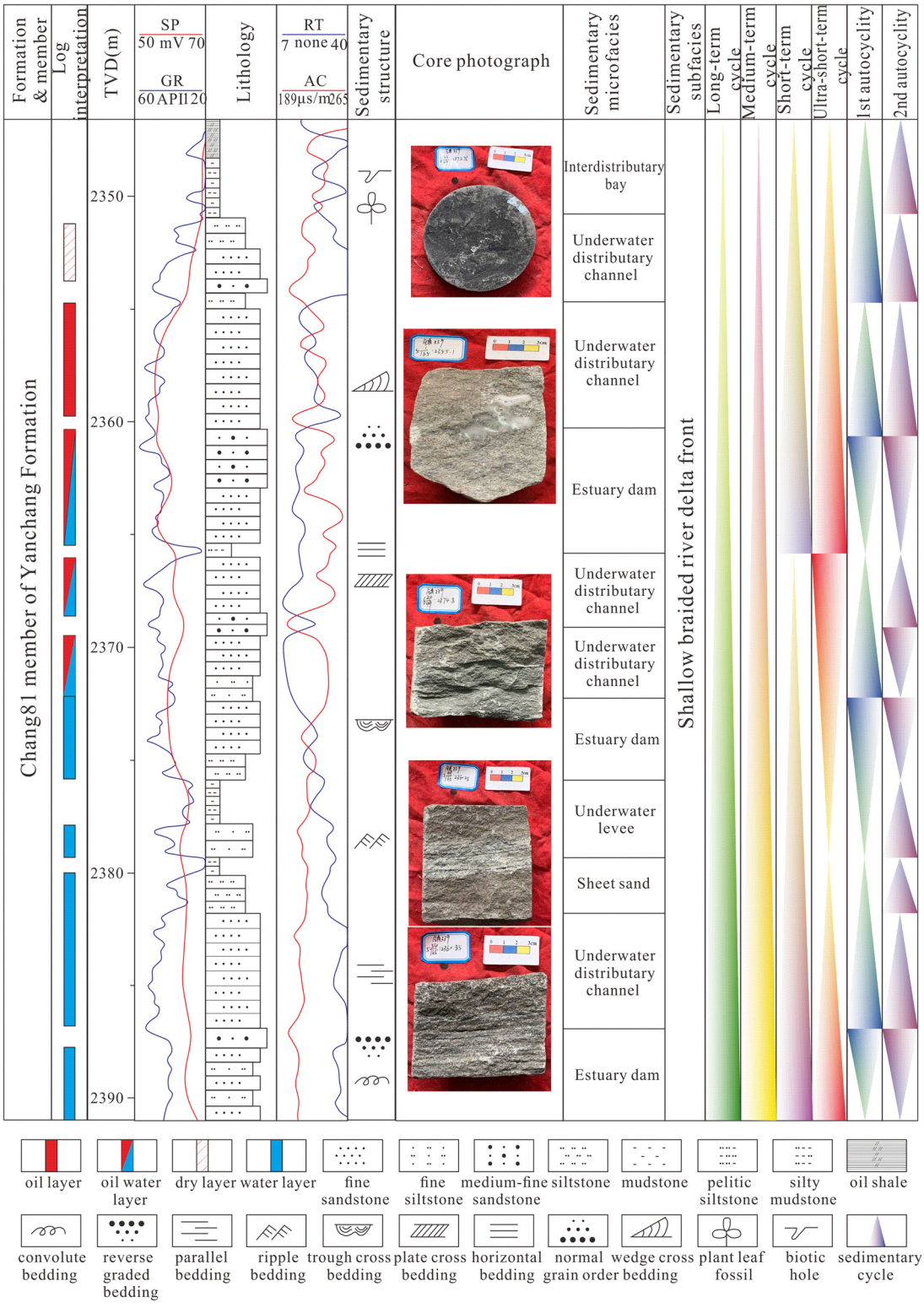

Figure 9: Base-level cycle identification and classification of single-well sequence architecture of well Z339.

Table 3: Classification and characteristics of monogenic sandbody-level architectural elements

Name of architectural element	Underwater distributary channel	Estuary dam	Underwater natural levee	Front sheet sand	Interdistributary bay fine-grained sedimentary unit
Autocyclicity type	Normal cycle	Reverse cycle	Normal cycle	Normal cycle	Compounded
Lithofacies	Gm, Sl, Sh	Sl, Fsc	Sl, Fsc, Fl	Fsc	Fl
Delta front phase	Upper, middle and lower	Middle	Upper, middle and lower	Middle and lower	Upper, middle and lower
Quantity variation	Large-moderate-small	None-moderate-none	Small-moderate-large	None-small-moderate	Small-moderate-large
Cyclicality	Long	Relatively long	Relatively short	Short	Indistinct
Hydrodynamic condition	Strong	Relatively strong	Relatively weak	Relatively weak	Extremely weak
A/S	Large	Relatively large	Relatively small	Small	Extremely small
Logging characteristics	Mid-to-high amplitude serrated bell or box shape, with abrupt changes at the top and bottom	Mid-to-high amplitude serrated funnel shape, with gradual change at the bottom, and abrupt change at the top	Low amplitude serrated bell shape, with gradual change at the top, and abrupt change at the bottom	Mid-to-low- amplitude serrated finger shape, with abrupt contacts at the top and bottom	Low amplitude serrated linear shape, partially interspersed with mid-to-low- amplitude finger shape
Logging shape	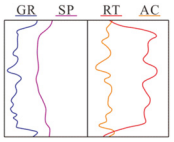	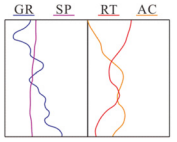	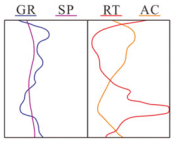	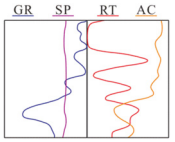	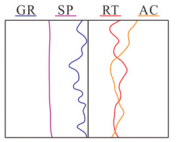
Width	250–650 m	180–450 m	100–210 m	180–370 m	Not measured
Thickness	2.3–8.5 m	1.5–6.7 m	0.8–4.1 m	0.5–3.5 m	Not measured
W/T ratio	30–280	27–300	24–263	51–740	Not measured

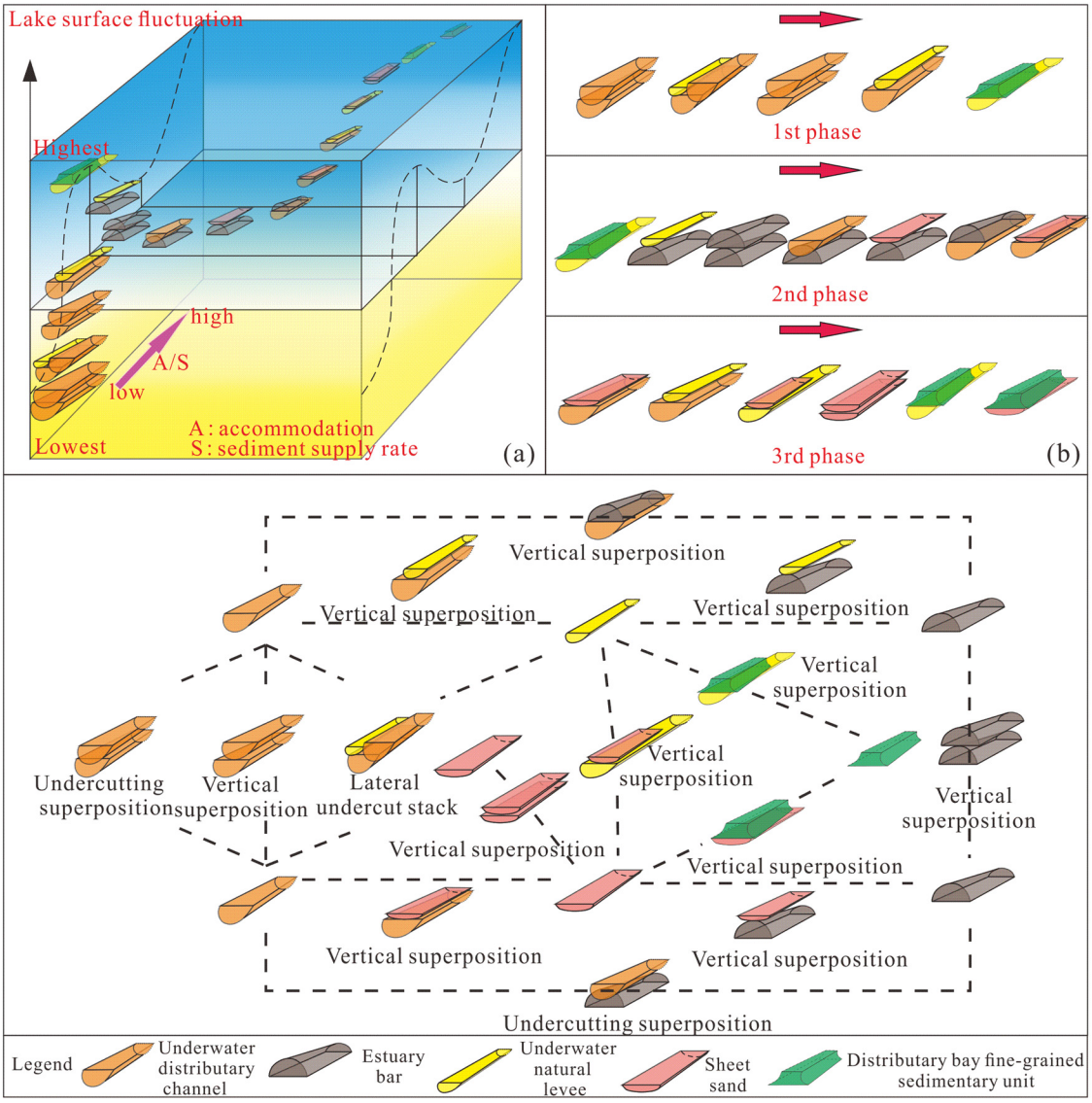

Figure 10: Classification of vertical superposition patterns of single sandbody architectural elements in the study area. (a) 14 major types of vertical superposition patterns during lake surface fluctuating; (b) three delta front phases of architectural evolution.

allocyclicity to autocyclicity architectural element classification is accomplished.

6 Discussion

6.1 Stratigraphic process-response sedimentary dynamics

By regarding the ultrashort-term cycles as the genetic stratigraphic units, we consider that the first ultrashort-term base-level cycle in the study area is an upwardly deepening asymmetric cycle with little accommodation ($A/S < 1$).

Initially, the lake level was extremely low and tended to increase slowly. Later, the lake-level rise accelerated gradually to a medium water level and then decelerated slowly to medium and high levels. Under the condition of a low water level, the sandbodies accumulated rapidly and formed a composite underwater distributary channel with a cut-and-stack style. From the middle of the channel to the flank, the development of underwater levees and an underwater distributary bay can be seen.

The second ultrashort-term base-level cycle is an upwardly shallowing asymmetrical cycle with high accommodation ($A/S > 1$). The lake level fell rapidly and then

slowly to a medium level from a medium to high level. Due to the decrease in base level, the sedimentary process became a weak aggradation–progradation process, and the hydrodynamics increased from a low level to a moderate level.

With the decrease in flow velocity, unloading occurred at the estuary, and an estuary bar with an inverse grain sequence formed. The underwater distributary channel sandbodies and mouth bar sandbodies began to be deposited. At the same time, front sheet sandbodies were produced by erosion of the estuary bar.

The third ultrashort-term base-level cycle is an upwardly deepening asymmetrical cycle with high accommodation (A/S ≫ 1). The lake level rose rapidly and then slowly to the highest value (maximum flooding surface of Chang 7) from the medium water level.

The underwater distributary channel sandbodies are still visible in the lithofacies, but they quantitatively decline, and most are in an isolated form. In the middle and later stages of the middle delta front, the sediments of the estuary bar suffered erosion and gradually disappeared. They disappeared due to their instability under shallow-water conditions.

6.2 Types and characteristics of single sandbody architectural elements

Taking into consideration the comprehensive logging responses, five types of monogenic sandbody architectural elements are identified in the study area, namely, underwater distributary channels, estuary dams, underwater natural levees, sheet sands, and interdistributary bay fine-grained sedimentary units (Table 3).

6.3 Vertical superposition patterns of architectural elements changing with base-level cycles

On the basis of sedimentogenesis analysis, 14 major types of vertical superposition patterns are screened for architectural elements (Figure 10a).

During the upper delta front phase of architectural evolution (Figure 10b), the lake level was rather low, and despite slight elevations in the later period, the hydrodynamics were relatively strong overall. The underwater

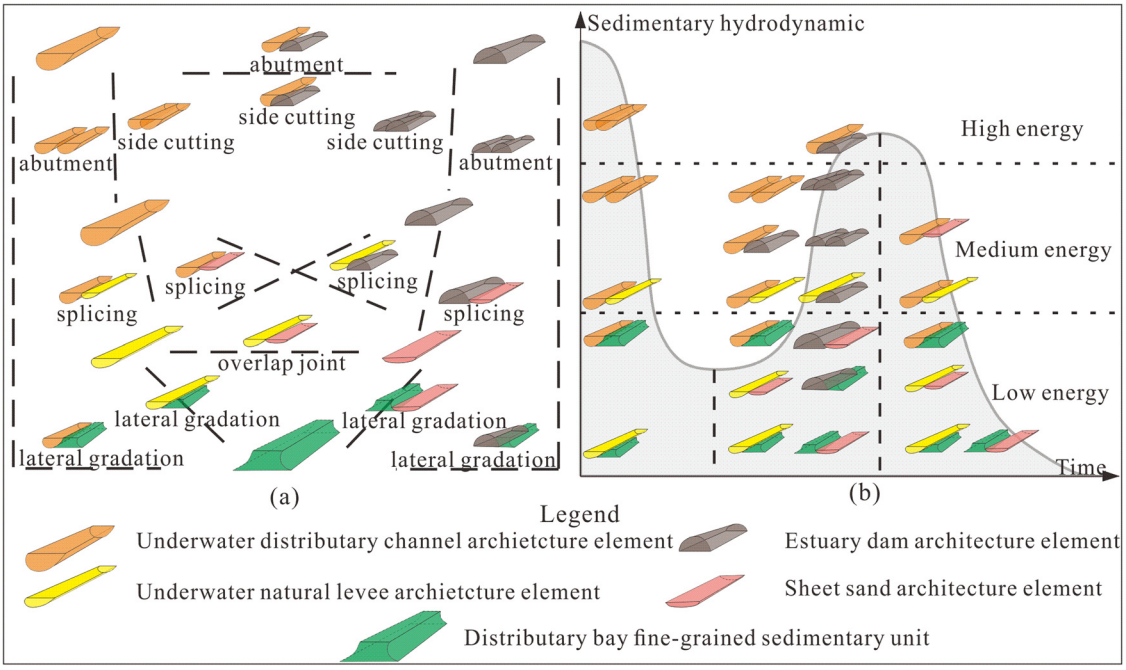

Figure 11: Classification of lateral contact patterns between single sandbody architectural elements in the study area. (a) The combinations of lateral contact relationships between various architectural elements; (b) the lateral contact patterns changes with the architectural evolution.

distributary channel elements are the primary type of sandbody architectural elements, while the interdistributary bay fine-grained sedimentary units and underwater natural levee elements are relatively rare. Regarding the vertical superposition patterns of single sandbody architectural elements, vertical and lateral undercutting stacks of underwater distributary channels prevail, both of which are stacking patterns in a strong hydrodynamic environment.

During the middle delta front phase of architectural evolution, the overall water level was high, the sedimentary hydrodynamics were severely weak, and the sedimentary strength declined in a gradual manner. The vertical superposition patterns of single sandbody architectural elements are observed mainly around the estuary dam and underwater distributary channel elements, which include the vertical superposition of estuary dams with underwater natural levees and the vertical superposition of estuary dams.

During the lower delta front phase of architectural evolution, the lake level rose again, and the maximum flooding period of Chang 7 was reached at the end of this phase. Thus, the lake level rose to the maximum in this phase, the energy of the sedimentary environment was low, and the hydrodynamic force weakened gradually to the minimum. The major types of sandbody architectural elements include a reduced number of underwater distributary channels, a slightly increased number of underwater natural levees, and significantly increased numbers of front sheet sands and interdistributary bay fine-grained sedimentary units. All the vertical superposition patterns of single sandbody architectural elements are types with weak sedimentary hydrodynamics.

6.4 Lateral contact patterns of architectural elements changing with base-level cycles

The lateral contact pattern of single sandbody architectural elements is the epitome of the horizontal distribution of sedimentary microfacies. Different types of single sandbody architectural elements are affected by different hydrodynamic forces in the sedimentary environment, showing different lateral contact patterns, which can reflect the sedimentary evolution process (Figure 11).

In Figure 11a, the combinations of lateral contact relationships between various architectural elements in the study area are illustrated and are classified primarily into side cutting, lateral contact, and abutment. In the side cutting condition, two single sandbodies have a strong lateral communication relationship; whereas in the abutment condition, the communication relationship between two single sandbodies is weak. Furthermore, the lateral contact relationships between single sandbody architectural elements are prominently affected by the sedimentary hydrodynamics.

The upper front phase of the shallow braided river delta experienced a strong-to-weak transition process in terms of the hydrodynamics. The side cutting of underwater distributary channels developed during the high-energy depositional stage with strong hydrodynamics in the middle of the main channels. At the intersections and junctions of river channels, two types of lateral contact relationships with medium hydrodynamics developed, namely, the abutment between underwater distributary channels and the abutment of underwater distributary channels with underwater natural levees. At sites such as the channel flanks or the branch channel sides, lateral contact relationships with weak hydrodynamics developed, such as the abutment of underwater distributary channels with interdistributary bay fine-grained sedimentary units and the abutment of underwater natural levees with interdistributary bay fine-grained sedimentary units.

The middle front phase of the shallow braided river delta undergoes a weak-to-strong transition process in terms of the hydrodynamics, and many types of lateral contact relationships are present. Initially, the hydrodynamic force was weak, and a range of lateral contact patterns developed, including sheet sands, underwater natural levees, and interdistributary bay fine-grained sedimentary units. Later, the hydrodynamics increased gradually to moderate levels, and a range of lateral contact relationships dominated by estuary dams and underwater distributary channels developed. Afterward, the hydrodynamics reached their strongest point in this phase, and the side cutting lateral contact pattern developed between underwater distributary channels and estuary dams in a high-energy environment.

The lower front phase of the shallow braided river delta exhibited a strong-to-weak transition process in terms of the hydrodynamics. After the disappearance of estuary dams, lateral contact relationships no longer formed in the high-energy environment. Under medium hydrodynamic conditions, abutting lateral contacts developed between the underwater distributary channels and the underwater natural levees and sheet sands. Although the lateral contact relationships developed in a low-energy environment inherited from the previous two phases, they decreased in number slightly, which reflects a significant reduction in hydrodynamic intensity (Figure 11b).

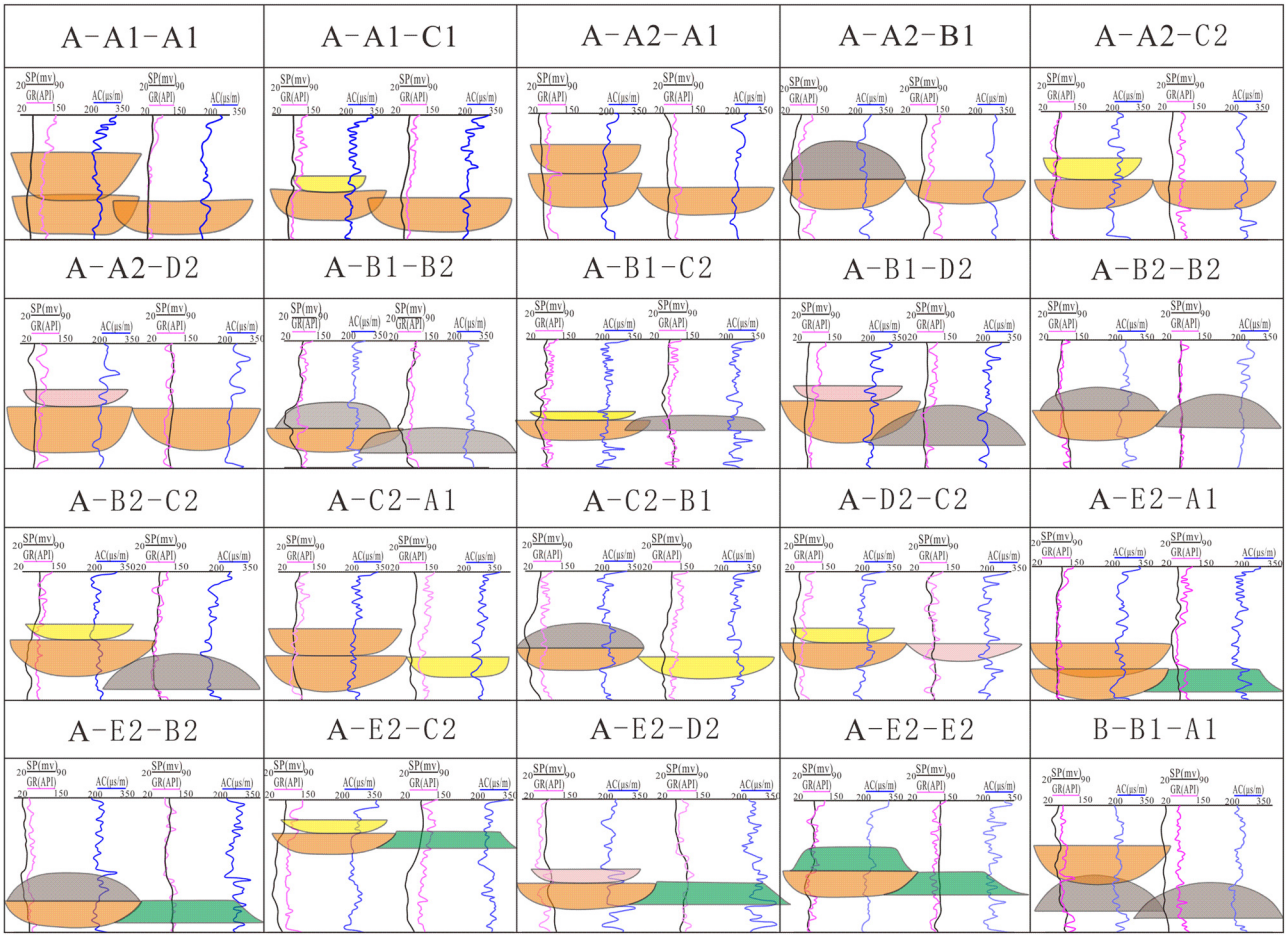

Figure 12: Spatial combination pattern classifications of architectural elements.

6.5 Classification and characteristics of spatial combination patterns of single sandbody architectural elements

By integrating the vertical superposition patterns with the lateral contact relationships, a variety of spatial combination pattern classifications are formed for the architectural elements. Based on the architectural element identifications with comprehensive logging responses, the number of spatial combination patterns, which are developed on several trunk profiles, is counted in the study area. According to the findings, there are 20 major types of spatial combination patterns (Figure 12).

Note: These patterns are expressed in the form of M-N1(N2)-P1(P2) or M-N2-P2 (where M denotes the basal single sandbody architectural element, N1 denotes the single sandbody architectural element in side cutting contact with M, N2 denotes the single sandbody architectural element in abutting contact with M, P1 denotes the single sandbody architectural element in a vertical tangential overlapping pattern with M, and P2 denotes the single sandbody architectural element in a vertical superposition pattern with M; furthermore, A represents the underwater distributary channel architectural element, B represents the estuary dam architectural element, C represents the underwater natural levee architectural element, D represents the front sheet sand architectural element, and E represents the interdistributary bay fine-grained sedimentary unit).

6.6 Comprehensive evaluation of spatial combination patterns of single sandbody architectural elements

After considering the sedimentary environment and development status, these spatial combination patterns are classified into levels I, II, III, and IV by integrating parameters, such as the geometric attributes, logging cycle

Architecture combination level	Architecture spatial combination relationship	Spatial relationship diagrammatic sketch	Width range	Thickness range	Well response	Allocyclicity	Porosity	Architectural position	Average permeability	Water-flooding	Displacement efficiency	remaining oil distribution
I Level	A-A1-A1	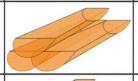	455-1236m	5.5-12.2m			7.5%	Main interchange of underwater distributary channel	1.85mD	95.4%	70.5%	
I Level	A-A2-A2	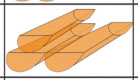	613-1548m	3.8-11.7m			7.4%	Main underwater distributary channel	1.62mD	72.3%	65.7%	
I Level	A-B1-B2	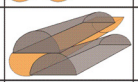	306-943m	3.4-9.5m			6.5%	High water level river mouth dam intersection	1.24mD	81.0%	60.2%	
I Level	A-A2-B2	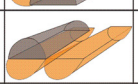	426-1021m	3.5-9.0m			7.1%	High water level river crossing	1.49mD	67.2%	57.5%	
I Level	B-B1-A1	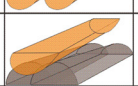	268-812m	3.1-7.2m			5.8%	River mouth dam begins to erode	1.18mD	55.4%	52.7%	
II Level	A-A1-C2	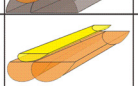	324-607m	2.4-6.0m			7.2%	Transition area from main river to edge	1.09mD	48.9%	48.0%	
II Level	A-C2-A1	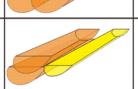	240-478m	3.2-8.0m			5.4%	Main underwater distributary channel flank	1.12mD	52.1%	50.3%	
II Level	A-B1-D2	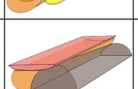	310-583m	2.4-5.8m			4.7%	The river mouth dam is gradually eroded	0.87mD	42.3%	46.1%	
II Level	A-B1-C2	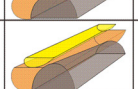	291-564m	2.3-6.1m			5.2%	Middle to side transition of medium hydrodynamic	0.90mD	45.0%	44.9%	
II Level	A-B2-B2	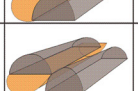	325-642m	3.1-7.5m			4.3%	At the front of the river, the mouth bar begins to develop	0.82mD	55.4%	48.2%	
III Level	A-E2-A1		226-393m	3.4-7.4m			4.0%	Flank of main channel at lower water level	0.78mD	53.1%	46.4%	
III Level	A-A2-C2		295-602m	2.4-5.9m			5.6%	Edge of underwater distributary channel intersection	0.71mD	38.5%	41.9%	
III Level	A-A2-D2		301-590m	2.7-6.0m			3.7%	Middle water level riverside	0.65mD	35.7%	40.4%	
III Level	A-B2-C2		271-569m	2.4-5.7m			3.8%	Middle water level branch channel	0.60mD	30.1%	35.4%	
III Level	A-C2-B2		214-456m	2.8-6.8m			4.0%	Branch channel	0.62mD	36.3%	37.1%	
IV Level	A-E2-B2		205-384m	3.1-6.5m			3.1%	Edge of branch river	0.59mD	35.4%	36.7%	
IV Level	A-D2-C2		226-470m	2.3-4.9m			3.1%	The branch channel of the river mouth dam disappearing	0.56mD	28.7%	31.9%	
IV Level	A-E2-C2		194-349m	2.1-4.5m			4.2%	High water level branch river flank	0.51mD	25.8%	28.2%	
IV Level	A-E2-D2		201-368m	2.0-4.2m			3.1%	Front of high water level branch channel	0.47mD	24.9%	27.0%	
IV Level	A-E2-E2		147-345m	1.9-3.6m			4.3%	Front end of high water level branch channel	0.43mD	17.8%	21.4%	

Figure 13: Comprehensive evaluation of the spatial combination patterns of the single sandbody architectural elements.

characteristics, distribution ratio, permeability, development position, water flooding, displacement efficiency, and remaining oil distribution position (Figure 13).

Among the level I spatial combinations, type A-A1-A1 occupies the largest proportion and features the largest thickness, a high average permeability, a high degree of

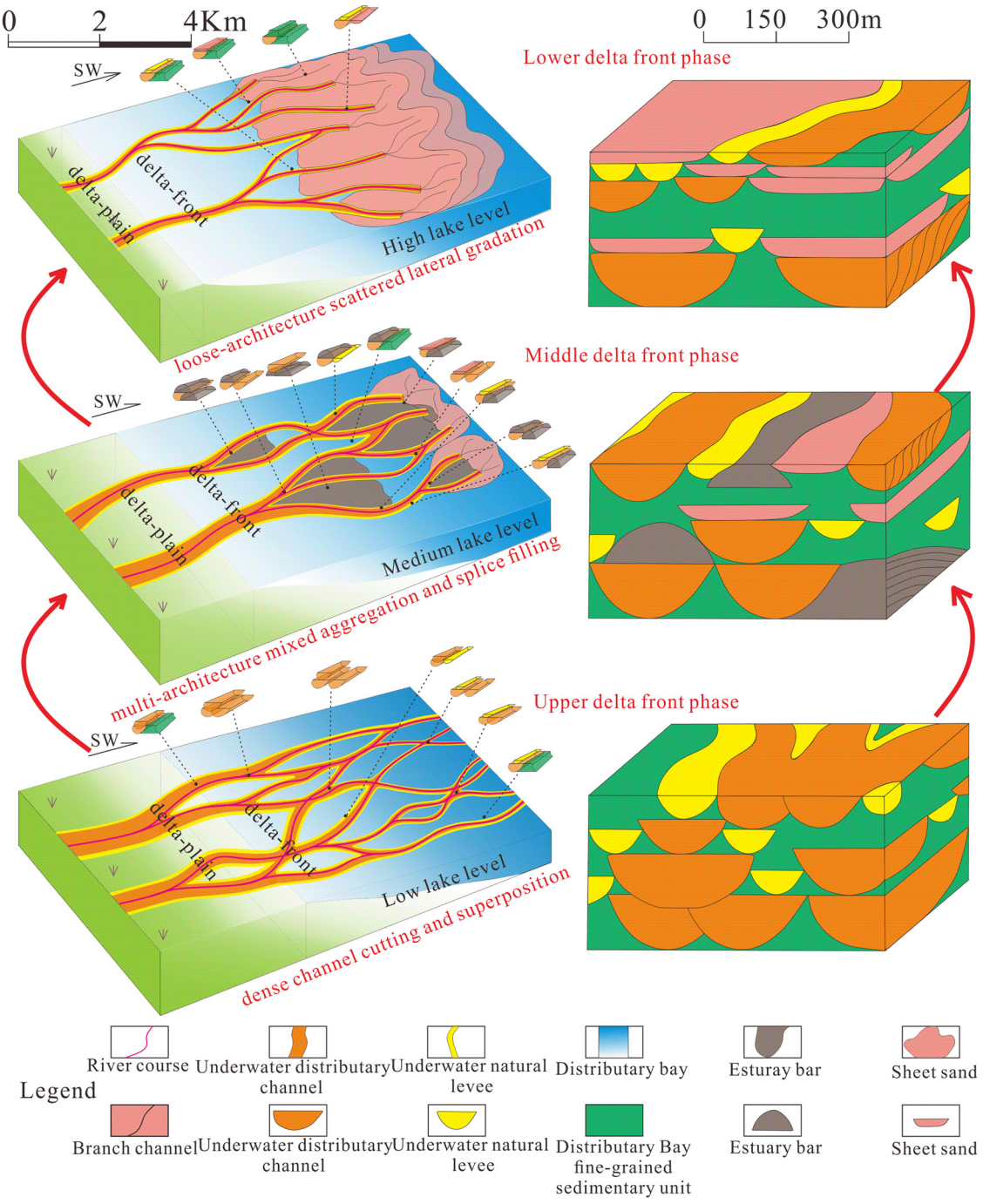

Figure 14: Evolution of spatial combination models between sandbody architectural elements.

water drive production, and little remaining oil. This reflects the spatial combination pattern of dominant sandbody connectivity resulting from the main channel sedimentation. Type A-A2-A2 also accounts for a large proportion but actually has very weak spatial connectivity. Hence, there is a substantial distribution of remaining oil. The types A-BA-B2 and A-A2-B2 are also combination patterns with relatively broad spatial connectivity and a substantial distribution of remaining oil. Relevant displacement efficiencies, however, are markedly lower in these two types than in the previous two types. Type B-B1-A1 is the product of the peak development of estuary dams, when the sedimentary hydrodynamics were relatively strong despite the small proportion of development.

Thus, the permeability is maintained at a relatively high level, and the remaining oil distribution is substantial as well.

Among the level II spatial combinations, both A-A1-C2 and A-C2-A1 are types with strong within-channel deposition, so the average permeability is also high. Types A-B1-D2 and A-B1-C2 represent the side cutting developmental period of estuary dams and underwater distributary channels, where the hydrodynamics were relatively strong. Because of good lateral connectivity, there is little remaining oil. A-B2-B2 is a type with favorable sandbody conditions but poor connectivity.

Among the level III spatial relationships, the combination patterns between underwater distributary channels and estuary dam sandbodies remain the major types. Although A-E2-A1, A-A2-C2, and A-A2-D2 are all combination patterns between underwater distributary channel sandbodies, the overall hydrodynamics were weak, the distribution areas are small, and the displacement index is very low. Types A-B2-C2 and A-C2-B2 are the combination patterns between underwater distributary channels and estuary dams and are associated with even weaker hydrodynamics than the previous combinations, and their physical properties are reduced.

Among the level IV patterns, A-E2-B2 is the most dominant relationship. Other types, including A-D2-C2, A-E2-C2, A-E2-D2, and A-E2-E2, are all combination types of weak hydrodynamic sediments that are developed under branch channels. In the current evaluation criteria, there is no potential for subsequent development.

6.7 The single sandbodies architectural evolution models

The sedimentary system of the shallow braided river delta front in the study area is subdivided according to the three time-stratigraphic units formed by the three ultra-short-term cycles into the upper front, middle front, and lower front phases. Then combined with the development status of single sandbody architectural elements identified in various phases and the research results of their spatial combination patterns, the sandbody architectural models and their evolution law are derived within these phases (Figure 14).

The features of the upper delta front architectural combinations are summarized as dense channel cutting and superposition. The primary architectural elements are underwater distributary channels, most of which are in a dense side cutting superposition pattern. Several distributary channels extend rapidly forward and interweave.

The features of the middle delta front architectural combinations are summarized as multiarchitecture mixed aggregation and splice filling. The coexistence of underwater distributary channels and estuary dams prevailed in this phase. The extent of the underwater distributary channel was shortened, and the mouth bar developed into fans. Small leafy sheet sand can be seen at the distal end of the delta. The connectivity of the distributary channels is reduced, and the channels are separated from each other. The mixing degree of various architectural elements is relatively high.

The features of the lower delta front architecture combinations are summarized as a loose architecture with scattered lateral gradation. Underwater distributary channels remained the dominant architectural element in this phase. In addition, various architectural elements were loosely superimposed, and their combinations formed a lateral gradation. In the early stage of this stage, the estuarine bar was generally washed out. The sheet sand began to be deposited in succession, and the branching channels were embedded in it, forming a loose pattern as a whole.

7 Conclusions

(1) Combined with the previous research results, the results of this study suggest that the study area featured a shallow lake depth and obvious delta front sedimentary characteristics.
(2) The allocyclicity is classified by using the sequence interface and lithofacies' sequence, and three ultra-short-term base-level cycles were identified in an outcrop along the Rui River. Then the Chang 8_1 Formation is divided into three sedimentary evolution stages: upper delta front, middle delta front, and lower delta front.
(3) Based on well data, the autocyclicity is divided, and five types of architectural elements at the microfacies scale are identified, which are equivalent to the fourth-order architectural elements of Miall.
(4) According to the lake-level change, the vertical overlap pattern and lateral contact pattern of architectural elements in each evolution stage were studied. Twenty main spatial combination patterns were formed, of which the first and second types have great development potential.

(5) The architectural evolution model mainly reflects that the geometry and connectivity of the underwater distributary channel are gradually weakened. However, the spatial combination patterns of underwater distributary channels and other architectural elements are closer.

Acknowledgments: This work was supported jointly by the National Natural Science Foundation of China (grant No. 41802140), the national science and technology major project (grant No. 2016ZX05050006), the Shaanxi basic natural science research plan project (grant No. 2019JQ-257), and the Liu Baojun Geosciences Foundation (DMSM2019007).

Declaration of competing interests statement: All authors declare that they have no known competing financial interests or personal relationships that could have appeared to influence the work reported in this article.

References

[1] Gilbert GK. The topographic features of lake shores. Nature. 1885;34(873):269–70.
[2] Bogen J. Morphology and sedimentology of deltas in fjord and fjord vally lakes. Sediment Geol. 1983;36:245–67.
[3] Syvitski JPM, Farrow GE. Structures and processes in bayhead deltas: knight and bute inlet, British Columbia. Sediment Geol. 1983;36:217–44.
[4] Tye RS, Coleman JM. Evolution of Atchafalaya lacustrine deltas, south-central Louisiana. Sediment Geol. 1989;65:95–112.
[5] Fisk HN. Recent Mississippi river sedimentation and peat accumulation. In: Erneast Van Aelst, ed., Fourth congress pour lavancement des' studes de stratigraphic et de geologic ducarbonifere, Heerlen, compt Rendu; 1960.
[6] Postma G. An analysis of the variation in delta architecture. Terra Nova. 1990;2(2):124–30.
[7] Keumsuk LL, McMechan GA, Gani MR, Bhattacharya JP, Zeng XX, Howell CD. 3-D architecture and sequence stratigraphic evolution of a forced regressive top-truncated mixed-influenced delta, cretaceous wall creek sandstone, Wyoming, USA. J Sediment Res. 2007;77(4):284–302.
[8] Lemons DR, Chan MA. Facies architecture and sequence stratigraphy of fine-grained lacustrine deltas along the eastern margin of late pleistocene lake Bonnevelle, northern Utah and southern Idaho. AAPG Bull. 1999;83:635–65.
[9] Zhang L, Bao ZD, Dou LX, Zang DS, Mao SW, Song J, et al. Sedimantary characteristics and pattern of distributary channels in shallow water deltaic red bed succession: a case from the late cretaceous yaojia formation, southern Songliao basin, NE, China. J Pet Sci Eng. 2018;171:1171–90.
[10] Zhu XM, Zeng HL, Li SL, Dong YL, Zhu SF, Zhao DN, et al. Sedimentary characteristics and seismic geomorphologic responses of a shallow-water delta in the Qingshankou formation from the Songliao basin, China. Mar Pet Geol. 2017;79:131–48.
[11] Li JP, Liu H, Niu CM, Guo RB, Wang Y. Evolution regularity of the Neogene shallow water delta in the Laibei area Bohai Bay basin, northern China. J Palaeogeogr. 2014;3(3):257–69.
[12] Gao Y, Hu XY, Zeng DQ, Zhao XY, Jia Y, Yu QY, et al. Sandbody type and distribution characteristics of shallow-water delta in Shanimiao formation, Xinchang gas field, west Sichuan. Geoscience. 2019;33(6):1163–1173+1207.
[13] Deng QJ, Hu MY, Hu ZH. Depositional characteristics and evolution of the shallow water deltaic channel sand bodies in Fuyu oil layer of central downwarp zone of Songliao basin, NE China. Arab J Geosci. 2019;12(20):1–14.
[14] Wang MQ, Xie J, Zhang Q, Wang YJ, Duan YJ. Characteristics and sedimentary model of a reticular shallow-water delta with distributary channels: lower member of the Neogene Minghuazhen formation in the Bozhong area of the Huanghekou Sag, China. Arab J Geosci. 2019;12(9):154–66.
[15] Li CH, Zhao J, Yao GQ, Li WQ, Liu HB, Wang YH, et al. Sedimentary facies and model of gentle slope shallow-water braided river delta in the Jurassic Sangonghe formation, Yanqi basin, China. J Pet Explor Prod Technol. 2019;9(3):1883–96.
[16] Wu SH, Xu ZH, Li Z. Depositional architecture of fluvial-dominated shoal water delta. J Palaeogeogr (Chin Edn). 2019;21(2):202–15.
[17] Xu ZH, Wu SH, Liu Z, Zhao JS, Geng HL, Wu JC, et al. Sandbody architecture of the bar finger within shoal water delta front: insights from the lower member of Minghuazhen formation, Neogene, Bohai BZ25 oilfield, Bohai Bay basin, east China. Pet Explor Dev. 2019;46(2):322–33.
[18] Simon J, Beavington PV, Wright P, Barrnett A, Kennedy S, Covill M. Integration of static and dynamic data and high-resolution sequence stratigraphy to define reservoir architecture and flow units within a 'super giant' gas condensate and oil field, Kazakhstan. Mar Pet Geol. 2018;101:486–501.
[19] Gao S, Chen SM, Pu H, Gong L, Ma SZ, Luo QY, et al. Fine characterization of large composite channel sandbody architecture and its control on remaining oil distribution: a case study of alkaline-surfactant-polymer (ASP) flooding test area in Xingshugang oilfield, China. J Pet Sci Eng. 2019;175:363–74.
[20] Mitten AJ, Mullins J, Pringle K, Howell J, Clarke SM. Depositional conditioning of three dimensional training images: improving the reproduction and representation of architectural elements in sand-dominated fluvial reservoir models. Mar Pet Geol. 2020;113:104156.
[21] Zou CN, Zhao WZ, Zhang XY, Luo P, Wang L, Liu LH, et al. Formation and distribution of shallow-water deltas and central-basin sandbodies in large open depression lake basins. J Geol. 2008;82(6):813–25.
[22] Hui X, Zhao YD, Shao XZ, Zhang WX, Cheng DX, Luo AX. The geological conditions, resource potential, and exploration direction of oil in Ordos basin. Mar Pet Geol. 2019;24(2):14–22.
[23] Luo JL, Shi CN, Li B, Li ZX, Li J, Han YL, et al. Sediment sources of Chang 8 and Chang 6 in Yanchang formation around Ordos

basin and Xifeng area: evidence from rock geochemistry. Chin Sci (Ser D Earth Sci). 2007;20(2):19–28.
[24] Zhu XM, Deng XQ, Liu ZL, Sun B, Liao JJ, Hui X. Sedimentary characteristics and model of shallow braided delta in large-scale lacustrine: an example from Triassic Yanchang formation in Ordos basin. Earth Sci Front. 2013;20(2):19–28.
[25] Liu HQ, Li XB, Wan YR, Wei LH, Liao JB. Palaeogeographic and sedimentological characteristics of the Triassic Chang 8, Ordos basin, China. Acta Sediment Sin. 2011;29(6):1086–95.
[26] Miall AD. Architectural-element analysis: a new method of facies analysis applied to fluvial deposits. Earth Sci Rev. 1985;22(4):261–308.
[27] Miall AD. The geology of fluvial deposits: sedimentary facies, basin analysis and petroleum geology. Berlin, Heidelberg, New York: Springer-Verlag; 1996. p. 74–98.
[28] Miall AD. Reconstructing the architecture and sequence stratigraphy of the preserved fluvial record as a tool for reservoir develop-ment: a reality check. AAPG Bull. 2006;90:989–1002.
[29] Diao F, Wen ZG, Zou HY, Li N. Sedimentary characteristics of shallow-water deltas in Chang 8 oil bearing interval in eastern Gansu, Ordos basin. Earth Sci J China Univ Geosci. 2013;38(6):1289–98.
[30] Liu ZL, Zhu XM, Liao JJ, Chen J. Sequence stratigraphy and genesis of sand bodies of the upper Triassic Yanchang formation in the southwestern margin of Ordos basin. Earth Sci Front. 2013;20(2):1–9.
[31] Wu SH, Ji YL, Yue DL, Yin SL. Discussion on hierarchical scheme of architectural units in clastic deposits. Geol J Chin Univ. 2013;19(1):12–22.